Phosphorescence and Optically Detected Magnetic Resonance of HIV-1 Nucleocapsid Protein Complexes with Stem−Loop Sequences of the Genomic Ψ-Recognition Element†

August H. Maki,*,‡ Andrzej Ozarowski,‡ Ajay Misra,‡ Maria A. Urbaneja,§ and José R. Casas-Finet§

Department of Chemistry, University of California, Davis, California 95616, and AIDS Vaccine Program, SAIC-Frederick, National Cancer Institute-Frederick Cancer Research and Development Center, Frederick, Maryland 21702-1201

Received August 24, 2000; Revised Manuscript Received November 29, 2000

ABSTRACT: The binding of NCp7, the nucleocapsid protein of human immunodeficiency virus type 1, to oligonucleotide stem−loop (SL) sequences of the genomic Ψ-recognition element has been studied using fluorescence, phosphorescence, and optically detected magnetic resonance (ODMR). RNA SL2, SL3, and SL4 constructs bind with higher affinity than the corresponding DNAs. G to I substitutions in the SL3 DNA loop sequence lead to reduced binding affinity and significant changes in the triplet state properties of Trp37 of NCp7, implicating these bases in contacts with aromatic amino acid residues of the zinc finger domains of NCp7, in agreement with the NMR structure of the 1:1 complex of NCp7 and SL3 RNA [DeGuzman, R. N., Wu, Z. R., Stalling, C. C., Pappaladro, L., Borer, P. N., and Summers, M. F. (1998) *Science 279*, 384−388]. The NCp7 to SL binding stoichiometry is 2:1 for intact SL sequences but is reduced to 1:1 for SL variants with an abasic or hydrocarbon loop. It is proposed that $\Delta D/\Delta E_{0,0}$, where ΔD is the change in the zero-field splitting D parameter and $\Delta E_{0,0}$ is the shift of the tryptophan phosphorescence origin, provides a measure of aromatic stacking interactions with nucleic acid bases. Values on the order of 10^{-5} indicate significant stacking interactions, while values closer to 10^{-6} result from interactions not involving aromatic stacking. Binding of NCp7 to oligonucleotide substrates produces shortened Trp37 triplet state lifetimes by enhancement of k_x and an increase of the relative value of P_x, the intersystem crossing rate to the T_x sublevel. These effects are attributed to a reduction in the degree of electronic symmetry of Trp37 in the complexes. Guanine and adenine triplet states produced by optical pumping of SL3 DNA are characterized. We find, as with tryptophan, that $|D| < 3|E|$.

Human immunodeficiency virus type 1 (HIV-1)[1] belongs to the lentivirus subfamily of retroviruses. Retroviruses utilize RNA as their genomic message and package two plus strands of genomic RNA into the virion (*1*). Genome packaging is directed by a gag polyprotein that is produced in the host cell during late stages of the infectious cycle. After budding from the cell, retroviruses typically undergo morphological rearrangements (maturation) during which the gag polyprotein is cleaved by the viral protease into several smaller proteins. During infection, the virus delivers its genomic message to the cell as a nucleoprotein complex that includes RNA, reverse transcriptase (RT), integrase (IN), and the viral nucleocapsid (NC) protein. RT transcribes the genomic RNA to double-stranded proviral DNA whose integration into the host genome is catalyzed by IN (*2*). The NC protein is a nucleic acid binding protein that has several roles in the viral replication cycle (*3*). It is involved in reverse transcription, retroviral assembly, and RNA packaging. As part of the gag polyprotein, the NC protein initiates genomic RNA encapsidation through recognition of a packaging signal. In HIV-1, the packaging signal (Ψ-site) is a ca. 120-nucleotide region of the unspliced viral RNA that is located between the 5′ long terminal repeat and the *gag* initiation codon (*4*). The mature virus contains about 2500 copies of the NC protein bound to two RNA strands, each composed of about 9000 nucleotides, about 7 nucleotides per NC protein (*5*). In this function, the NC protein exhibits non-sequence-specific binding to single-stranded RNA and promotes the condensation of RNA into the core structure.

NC proteins of all known retroviruses (except members of the spumavirus class) contain one or two copies of a conserved amino acid sequence consisting of 10 variable amino acids (X) and 4 invariant ones (Cys-X_2-Cys-X_4-His-X_4-Cys). The invariant residues coordinate a zinc ion through histidine imidazole and cysteine thiolates, forming CCHC-

† This publication was made possible by Grant ES-02662 from the National Institute of Environmental Health Sciences (A.H.M.) and by National Cancer Institute Contract N01-56000 (J.R.C.-F.). Its contents are solely the responsibility of the authors and do not necessarily reflect the views of the NIEHS or NCI, NIH.

* To whom correspondence should be addressed. Telephone: (530) 752-6471. Fax: (530) 752-8995. E-mail: maki@chem.ucdavis.edu.

‡ University of California.

§ National Cancer Institute-Frederick Cancer Research and Development Center.

[1] Abbreviations: BrU, 5-bromouracil; D and E, zero-field splitting parameters; $E_{0,0}$, phosphorescence 0,0-band energy; EA, electron affinity energy; EEDOR, electron−electron double resonance; HIV-1, human immunodeficiency virus type 1; IP, ionization potential; ISC, intersystem crossing; MIDP, microwave-induced delayed phosphorescence; NC, nucleocapsid; NCp7, nucleocapsid protein of HIV-1; n_i^0, relative steady state population of T_i; ODMR, optically detected magnetic resonance; P_i, relative populating rate of T_i; SL, stem−loop; SLR, spin−lattice relaxation; SOC, spin−orbit coupling; T_i, triplet state sublevel with $i = x, y,$ or z; ZFS, zero-field splitting.

10.1021/bi002010i CCC: $20.00
Published on Web 01/12/2001

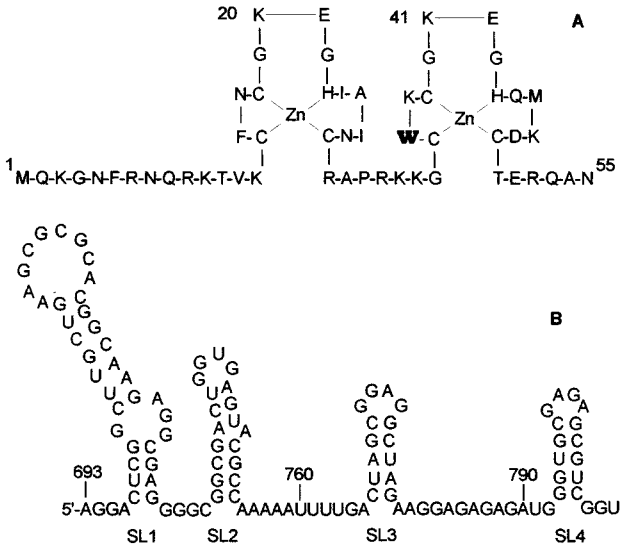

FIGURE 1: (A) Amino acid sequence of NCp7. (B) Base sequence and proposed secondary structure of Ψ-site RNA of HIV-1.

type zinc fingers (*6*, *7*) whose organized structures are essential for genome recognition. The variable residues (X) distinguish the CCHC-type zinc fingers associated with specific NC proteins, but they exhibit conserved features such as the placement of aromatic residues (Trp, Tyr, Phe, and His). Lentiviruses have two CCHC zinc fingers per NC protein, each containing an aromatic (Aro) residue (Cys-X-Aro-Cys-X_4-His-X_4-Cys). The NC protein of HIV-1 (NCp7) contains Phe in the first zinc finger and Trp in the second, while the simian immunodeficiency virus (SIV) NC protein (NCp8) contains Trp in both zinc fingers. Mutations that abolish zinc binding in NC protein lead to noninfectious virions that lack their genomes (*8*−*10*). Basic sequences surrounding the zinc finger domain in NC protein have also been implicated in RNA annealing activity (*11*) and virus infectivity (*12*). In general, zinc finger mutations of the NC protein produce virions that are replication-defective in vitro and in vivo (*13*, and references therein). Mutations of conserved hydrophobic residues within the CCHC zinc fingers can alter RNA packaging specificity (*14*). NC domain swapping experiments confirmed that the NC protein recognizes specifically the retroviral genomic RNA during RNA encapsidation (*15*).

In previous work, we have studied complexes of the 55-amino acid NCp7 (Figure 1A) with several oligonucloeotides and polynucleotides (*16*, *17*). Fluorescence titrations were carried out monitoring Trp37 to determine binding characteristics. Phosphorescence and optically detected magnetic resonance (ODMR) measurements were taken at cryogenic temperatures using Trp37 as a probe to further characterize the interactions of this residue in the complexes. In the work presented here, we have extended these measurements to complexes of NCp7 with stem−loop (SL) RNA and DNA constructs based on elements contained in the Ψ-site (Figure 1B). The structure of a 1:1 complex of NCp7 with a 20-nucleotide RNA construct based on SL3 has been determined recently using NMR (*18*).

MATERIALS AND METHODS

Materials. The NCp7 protein from HIV-1/MN was obtained as described previously (*16*). HPLC fractions containing NCp7 (identified by PAGE mobility, Western blotting, and N-terminal sequencing) were collected, pooled, and lyophilized. NCp7 was resuspended in the presence of excess Zn^{2+}, and its concentration was calculated on the basis of optical absorbance and amino acid analysis measurements. This solution was aliquoted into sterile polypropylene vials and relyophilized. Concentrations were determined spectrophotometrically using an ϵ_{280} of 5.7×10^3 cm^{-1} M^{-1}. Buffers and doubly distilled water were passed through a 0.22 μm sterile filter before use.

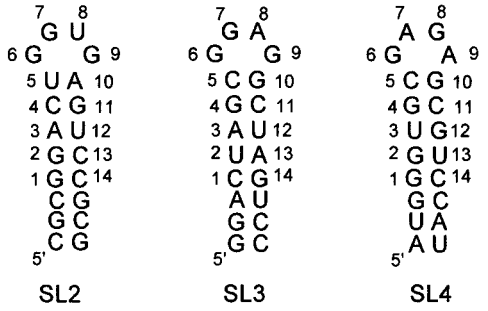

FIGURE 2: Base sequence of the SL2, SL3, and SL4 stem−loop fragments prepared for this work.

The SL2, SL3, and SL4 20-mer sequences used in these studies are shown in Figure 2. The RNA constructs were obtained from Midland Certified Reagent Co. (Midland, TX). The DNA constructs and the mutated SL3(G7I), SL3(G9I), SL3(G7I/G9I), and SL2(U8BrU) constructs were synthesized by either Gibco Life Technologies Inc. (Rockville, MD) or Midland Certified Reagent Co. DNA loop variants of SL3 were also synthesized. SL3(abasic)$_4$ consists of the SL3 stem sequence in Figure 2 but lacks the four loop bases which are replaced with an apurinic tether. SL3$(CH_2)_9$ consists of the SL3 stem sequence but has an *n*-nonane tether in place of the DNA tetraloop. These variants were obtained from Midland Certified Reagent Co. Self-complementary 14-mer DNA with the sequence 5′-dCATATGCGCATATG-3′ (ds-DNA) and "scrambled" 14-mer DNA with the sequence 5′-dAGCTTGAAACCTTG-3′ (ssDNA) were obtained from the Recombinant DNA Laboratory (SAIC-Frederick). These oligomers have the same overall base composition. Poly(A) was obtained as a lyophilized sample from Sigma.

Methods. Binding affinities of HIV NCp7 for the various DNA and RNA stem−loop sequences used in this study were obtained by monitoring its tryptophan fluorescence emission in the presence of varying concentrations of the lattice. Fluorescence measurements were carried out with a SPEX Fluoromax 2 spectrofluorimeter, exciting at 295 nm (1 nm bandwith) and monitoring emission at 356 nm (5 nm bandwith). Equilibrium binding isotherms were acquired at 25 °C, following stepwise additions of a stock solution of the 20-mer stem−loop sequences, or any of its modifications used through this study, to a 1 mL NCp7 sample (1 μM) in 10 mM sodium phosphate buffer (pH 7.0) placed in a Teflon-capped, dual-path length (0.4 cm × 1.0 cm) Suprasil quartz cell (Hellma Cells, Inc., Jamaica, NY). Readings were taken every 5 s for 2 min, averaged, and corrected for dilution and inner filter effects. NCp7 binding was monitored by the decrease in the initial fluorescence of the protein. The fractional saturation of the HIV NC protein was inferred from the ratio of observed quenching to maximal quenching (at saturation) for each of the nucleic acid stepwise additions.

The occluded binding site size (n) was derived from the extrapolation of the initial slope with the limiting fluorescence plateau in equilibrium binding isotherms. The stoichiometry of the binding was estimated using the n values. Binding affinities (K_{obs}) were calculated directly from a double-reciprocal plot of $1/[\text{nucleotide}]_{free}$ versus $1/\Delta F$ where ΔF reflects the quenching extent. Dividing the site size by the slope of the linear regression yields binding affinity.

Phosphorescence measurements were taken at cryogenic temperature (77, 4.2, or 1.2 K) using excitation from a 100 W high-pressure Hg arc lamp whose output was filtered by a monochromator with a 16 nm band-pass. ODMR experiments were carried out in zero applied magnetic field at 1.2 K. The phosphorescence and ODMR spectrometer, utilizing photon counting, has been described previously (*19, 20*). For these measurements, lyophilized samples were dissolved in 10 mM phosphate buffer (pH 7.2). Complexes were formed by adding an aliquot of the NCp7 solution to the nucleic acid solution and mixing for 10 min. Ethylene glycol (40% v/v) was added as a cryosolvent prior to spectroscopic measurements at low temperatures. Concentrations of NCp7 in the final solution ranged between 0.2 and 0.4 mM. The molar ratio of NCp7 to oligonucleotide was 1:1, but a small excess (∼10%) of the latter was used to ensure complete binding of NCp7. The sample volume was ∼50 μL contained in a 2 mm inside diameter Suprasil tube. Phosphorescence decay at 4.2 K was monitored at the 0,0-band wavelength of Trp37 and fitted by computer to two exponential components using a nonlinear least-squares procedure. The amplitude of the long-lived component (5−6 s), attributed to Trp37, is >90% of the total in NCp7−SL complexes. The minor component (1−2 s) is attributed to nucleic acid phosphorescence.

Although slow passage ODMR spectra were collected during optical pumping while scanning the complete microwave spectral range (using a rotating sector to select the phosphorescence), the bandwidths and band centers of individual transitions were obtained by analysis of delayed slow passage ODMR responses as described previously (*21*). As before, the band centers and widths of the assumed Gaussian-shaped bands were measured over a range of delays and sweep rates, and the results were averaged. The triplet sublevel kinetic parameters were obtained from global analysis of microwave-induced delayed phosphorescence (MIDP) transients, as previously described (*20*). The sum of the sublevel decay constants in the analysis was fixed at $3\langle k\rangle$, where $\langle k\rangle$ is the phosphorescence lifetime of Trp37 at 4.2 K, obtained as described above. Analysis of the delayed slow passage responses was carried out by two separate methods. In the previously employed method (*21*), the response is fitted to a set of empirical radiative and kinetic sublevel parameters. In a more recently developed method (*22*), the response is fitted to the actual kinetic and radiative parameters obtained from analysis of the independent MIDP data. Despite the many fewer fitting parameters in the newer method, both methods of analysis yield nearly the same band center frequency, ν_0, and bandwidth, $\nu_{1/2}$ (*22*). The zero-field splitting (ZFS) parameters of tryptophan, D and E, were calculated from the band center frequencies of the two most intense ODMR transitions, ν_0 ($D - E$) and ν_0 ($2E$). The ZFS parameters are related to the projections of the interelectron vectors along the principal axis directions by

$$D = \frac{3}{4}(\gamma\hbar)^2\langle({r_{12}}^2 - 3{z_{12}}^2)/{r_{12}}^5\rangle_{av} \quad (1)$$

$$E = \frac{3}{4}(\gamma\hbar)^2\langle({y_{12}}^2 - {x_{12}}^2)/{r_{12}}^5\rangle_{av} \quad (2)$$

where γ is the electron magnetogyric ratio and $\hbar$ is Planck's constant. The interelectron coordinates are averaged over the triplet state wave function. The principal z-axis is normal to the molecular plane of the indole moiety, while the x-axis is approximately normal to the 2−3 double bond (*23*).

EXPERIMENTAL RESULTS

Fluorescence Titrations. Addition of saturating amounts of nucleic acid ligands induced a dramatic quenching of the NCp7 tryptophan fluorescence. The maximum quenching observed (ΔF_{lim}) was >85% for all cases, showing the highest values among the intact stem−loop sequences for SL2 and SL3 RNAs (Table 1). Only the single-stranded oligo (the "scrambled" oligo) DNA induced a higher reduction (95−96%) of the protein fluorescence. Binding stoichiometries were calculated using the occluded binding site size, as has been mentioned in Materials and Methods. Two NCp7 molecules bound to one DNA or RNA stem−loop fragment of each sequence. However, when the four loop bases in SL3 were replaced either with a phosphodiester backbone, $SL3(abasic)_4$, or with an n-nonane tether, $SL3(CH_2)_9$, the stoichiometry dropped to one NCp7 per oligonucleotide (Table 1). The loss of one binding site when the loop bases are missing implies that they are directly involved in the formation of one of the two binding sites, the second site being the bases that are structured in the double-stranded stem. To probe whether NCp7 is capable of binding to a double-stranded nucleic acid, we used a self-complementary dsDNA. The titration of the nucleocapsid protein with dsDNA induced a quenching of 90% of the protein fluorescence, and nine base pairs were occluded by NCp7 at saturation. On this basis, our data correlate perfectly with a model in which two NCp7 molecules bind to different domains in the stem−loop sequence.

Binding affinities were determined directly from the titration experiments. Each RNA stem−loop sequence exhibited a higher affinity than its respective DNA counterpart (Table 1). The increase in K_{obs} is 2-, 4-, and 13-fold for SL4, SL2, and SL3 RNA, respectively. The higher affinity mirrors the greater extent of quenching when RNA stem−loop sequences were used to titrate NCp7. We carried out experiments in the presence of ethylene glycol (40%) so that the conditions resembled those of the buffer in which the ODMR measurements are performed. The presence of the cryoprotectant produced only a minor reduction in K_{obs} relative to the binding affinity in phosphate buffer.

The three-dimensional structure of NCp7 bound to SL3 RNA published by Summers, Borer, and co-workers (*18*) implicates the guanosine residues located in the loop in the stabilization of the complex. Thus, we studied the effect of single mutations of one or both of these bases on the affinity of NCp7 for those mutants. The substitution of either G7 or G9 of SL3 DNA (Figure 2) with inosine produced a similar loss of binding affinity relative to the canonical sequence. Moreover, the double substitution resulted in an even greater reduction in K_{obs}. The role played by the loop bases in

Table 1: Equilibrium Binding Constants

substrate	NCp7:oligo stoichiometry	ΔF_{lim} (%)	K_{obs}[a] (M^{-1})
SL2 RNA	2:1	94	6.7×10^8
SL3 RNA	2:1	95	1.3×10^9
SL4 RNA	2:1	94	8.7×10^7
SL2 DNA	2:1	90	1.8×10^8
SL3 DNA	2:1	91	1.0×10^8
SL3 DNA (40% EG)	2:1	93	3.8×10^7
SL4 DNA	2:1	94	4.0×10^7
SL3(G7I) DNA	2:1	89	5.1×10^7
SL3(G9I) DNA	2:1	90	5.3×10^7
SL3(G7I/G9I) DNA	2:1	90	3.0×10^7
$SL3(abasic)_4$ DNA	1:1	91	2.3×10^7
$SL3(CH_2)_9$ DNA	1:1	91	1.9×10^7
$SL2(abasic)_4$ DNA, A bulge	1:1	91	2.0×10^7

[a] The equilibrium binding isotherms were carried out in 10 mM sodium phosphate buffer (pH 7.0).

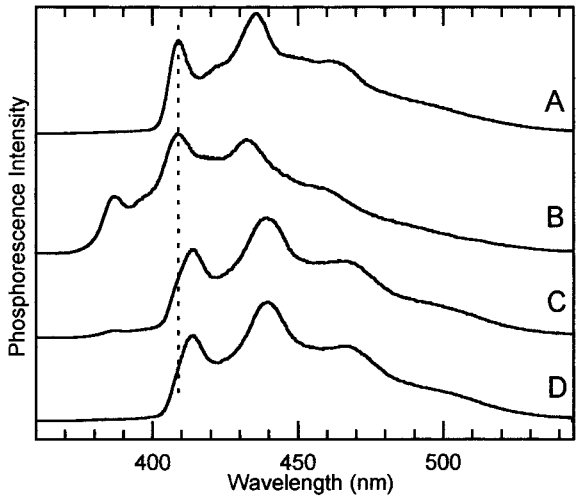

FIGURE 3: Phosphorescence spectra of (A) NCp7, (B) SL3 DNA, and (C and D) the 1:1 complex of NCp7 and SL3 DNA. Spectra A−C were recorded at 1.2 K, and spectrum D was recorded at 77 K.

stabilizing the complex was further assessed by removal of the purinic bases in the synthetic SL3 DNA sequence. The abasic SL3, where only the sugar−polyphosphate backbone is present in the loop region, binds with a 4-fold lower K_{obs} than the wild-type SL3 (Table 1). The binding stoichiometry is reduced to 1:1, as noted earlier. When the nucleotides in the loop were substituted with an *n*-nonane tether, the stoichiometry remains 1:1 and, although slight, a further reduction in binding affinity was observed. This finding shows that the phosphate backbone in the loops also plays a role in the stabilization of the complex.

Phosphorescence Spectra. The phosphorescence spectra of NCp7, SL3 DNA, and their equimolar complex measured at 1.2 K are shown in Figure 3. Also shown is the phosphorescence of the complex at 77 K. The emission of NCp7 is highly structured and characteristic of tryptophan (*24*). The 0,0-band is located at 409.6 nm, as reported previously (*17*). The SL3 DNA phosphorescence also is structured with a 0,0-band peak at ~385 nm. It can be seen in Figure 3C that at 1.2 K the emission of the complex is dominated by tryptophan phosphorescence but a DNA component, identified by a minor peak at ~385 nm, is present. At 77 K, however, the DNA component is completely quenched (Figure 3D). Complex formation between NCp7 and SL3 DNA leads to a noticeable red shift of the Trp37 0,0-band as can be seen by comparing trace A in Figure 3 with trace C or D in Figure 3. Similar red shifts of Trp37 were reported previously for NCp7 complexes with model poly- and oligonucleotides (*17*) and were attributed in most cases to aromatic stacking interactions. The results shown in Figure 3 are similar to those obtained with SL2 and SL4 DNA, and with each SL RNA, providing evidence that complex formation with each SL is effectively stoichiometric under our conditions. The 0,0-band peak wavelengths of Trp37 in these complexes are given in Table 2, as are the Trp37 phosphorescence lifetimes determined at 4.2 K. Spin−lattice relaxation is dominant at this elevated temperature, producing (aside from a minor initial transient) a single-exponential decay having the average sublevel decay constant. The reduction of the Trp37 triplet state lifetime in each of the complexes relative to that in free NCp7 provides further evidence for the involvement of this residue in complex formation.

ODMR of NCp7 and of SL3 DNA. Although we are primarily interested in the triplet state properties of Trp37 as revealed by ODMR experiments, the presence of some overlapping nucleic acid phosphorescence at 1.2 K (Figure 3C) could present a problem. The slow passage ODMR spectra of SL3 DNA and of NCp7 are shown as traces A and D of Figure 4, respectively. These spectra were obtained in the photostationary state during optical pumping using a rotating sector to eliminate fluorescence. The ODMR bands produced by free SL3 DNA originate from the triplet states of adenine and guanine, based on their ZFS (*25*) and by comparison with ODMR of poly(A) carried out in this work. The band center frequencies and bandwidths were obtained using delayed slow passage ODMR. These results and the ZFS *D* and *E* parameters of guanine and adenine are given in Table 3. The sublevel kinetic and radiative parameters were determined by global analysis of MIDP; these results are given in Table 3, as well. Our assignment of the ODMR transitions is based on assuming a positive value for both *D* and *E*. *D* is positive for $^3(\pi,\pi^*)$ electronic states of aromatic molecules (*26*) and requires T_z (*z*-axis normal to the molecular plane) to be the lowest energy level in zero magnetic field (provided $E < D$, which is assumed to be the case). The positive value assumed for *E* is arbitrary, but this choice requires that the energy of T_y is above that of T_x. Thus, the highest-frequency ODMR transition is $T_y \leftrightarrow T_z$. The lowest-frequency transition is either $T_x \leftrightarrow T_y$ or $T_x \leftrightarrow T_z$ depending on whether $D > 3E$ or $D < 3E$, respectively. The sublevel decay constant k_z is much smaller than k_x or k_y, since spin−orbit coupling between singlet states and the T_z sublevel is particularly unfavorable in $^3(\pi,\pi^*)$ electronic states (*27*, *28*). For both adenine and guanine, we can assign the lowest-frequency ODMR transition to $T_x \leftrightarrow T_z$ on the basis of the MIDP kinetics. This assignment also is possible to make qualitatively, since MIDP responses that involve T_z are the most persistent. Thus, for both adenine and guanine, $D < 3E$, as is the case for tryptophan.

It can be seen from Figure 4 that the low-frequency bands of adenine and of Trp37 at ~1.7 GHz overlap significantly. The results of EEDOR are shown in Figure 4. When the low-frequency band of guanine at ~1.1 GHz is saturated, all of its ODMR bands vanish (Figure 4B). In addition, when the low-frequency band of adenine at ~1.6 GHz is saturated,

Table 2: Triplet State Spectroscopic Properties of Trp37 in NCp7 and Its 1:1 Complexes with SL Structures[a]

		$\|D\| - \|E\|$		$2\|E\|$					
substrate	$\lambda_{0,0}$ (nm)[b]	ν_0 (GHz)	$\nu_{1/2}$ (MHz)	ν_0 (GHz)	$\nu_{1/2}$ (MHz)	$\|D\|$ (GHz)	$\|E\|$ (GHz)	lifetime (s)	$10^6\Delta D/\Delta E_{0,0}$
none	409.6	1.721(3)	51.5(9)	2.489(1)	122(3)	2.966(3)	1.244(1)	6.4	−
SL2 RNA	413.0	1.6663(5)	46(1)	2.556(1)	62(3)	2.944(1)	1.278(1)	5.0	3.6
SL3 RNA	413.7	1.645(1)	67.5(5)	2.56(1)	122(9)	2.925(5)	1.280(5)	5.1	5.6
SL4 RNA	414.8	1.659(2)	70(1)	2.53(1)	105(10)	2.924(5)	1.265(5)	5.2	4.6
SL2 DNA	413.3	1.6887(5)	56(1)	2.500(7)	80(7)	2.939(4)	1.250(4)	5.3	4.1
SL3 DNA	414.3	1.675(2)	65(2)	2.484(1)	114(7)	2.917(3)	1.242(1)	5.2	5.9
SL4 DNA	413.7	1.680(1)	73.8(3)	2.498(4)	133(5)	2.929(2)	1.249(2)	5.1	5.1
SL3(G7I) DNA	416.3	1.654(1)	54(3)	2.473(2)	120(4)	2.890(1)	1.236(1)	5.2	6.4
SL3(G9I) DNA	414.2	1.656(2)	82(5)	2.505(8)	171(11)	2.908(4)	1.252(4)	5.4	7.1
SL3$(CH_2)_9$ DNA	414.4	1.684(1)	73(3)	2.49(1)	133(19)	2.934(5)	1.250(5)	5.2	3.8
SL3(abasic)$_4$ DNA	414.1	1.6716(4)	79(2)	2.377(2)	163(5)	2.860(2)	1.188(1)	5.2	13.3
SL3(abasic)$_4$ DNA[c]	415.4	1.649(2)	68(1)	2.37(1)	150(20)	2.834(5)	1.185(5)	5.2	12.9
dsDNA	413.4	1.710(3)	75(1)	2.483(9)	120(16)	2.952(5)	1.242(5)	5.9	2.1
ssDNA	415.3	1.673(3)	65(2)	2.496(7)	112(3)	2.921(3)	1.248(4)	5.4	4.5
SL2(U8BrU) DNA	414.9	1.661(2)	65(1)	2.507(9)	136(10)	2.915(5)	1.254(5)	5.1	5.4

[a] The estimated error in the last digit is given in parentheses. [b] Trp37 0,0-band. The estimated error is ±0.4 nm. Excitation is at 297 nm except as noted. [c] Excitation is at 313 nm.

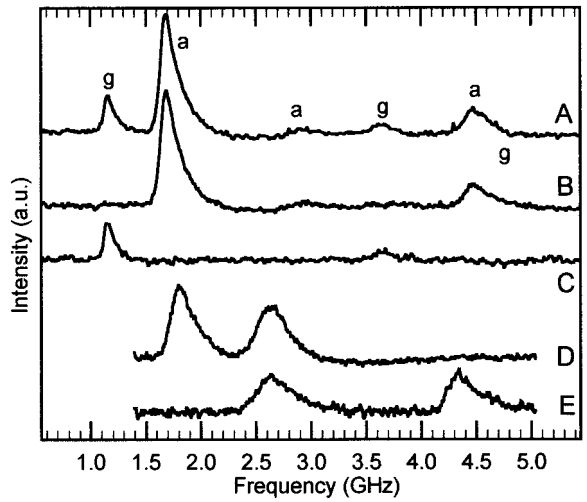

FIGURE 4: Steady state ODMR spectra of (A−C) SL3 DNA and (D and E) free NCp7. "a" and "g" mark the signals assigned to adenine and guanine, respectively. In spectrum B, the low-frequency guanine transition at 1.09 GHz is saturated, causing the disappearance of the guanine spectrum. In spectrum C, saturation of the low-frequency transition of adenine at 1.61 GHz removes all ODMR signals due to adenine. In spectrum E, saturation of the low-frequency $D - E$ transition of tryptophan at 1.72 GHz allows the observation of its $2E$ and $D + E$ transitions.

the entire adenine spectrum vanishes (Figure 4C). When the low-frequency band of Trp37 of NCp7 is saturated, however, its two higher-frequency bands are observed (Figure 4E). Thus, we can expect that when both adenine and Trp are present, saturating the low-frequency band region that is common to both triplet states will eliminate the photostationary state slow passage ODMR of adenine, leaving an EEDOR spectrum of Trp as seen in Figure 4E. The reason for the differing EEDOR behavior of guanine and adenine versus Trp is not relevant to this work, and will be discussed elsewhere. Guanine and adenine ODMR bands were detected in each of the other DNA and RNA SL sequences, but these were not studied in detail.

ODMR of NCp7 and Its SL Complexes. In a previous study of NCp7 complexes with model nucleic acids (*17*), it was observed that the effect of complex formation (and stacking interactions in particular) on the Trp37 sublevel kinetics produces stationary state sublevel populations that are nearly

Table 3: Triplet State Properties of Guanine and Adenine in SL3 DNA

	guanine[a]	adenine[b]	poly(rA)[c]
$D - E$ (GHz)	1.09(1)	1.613(1)	1.569(1)
$2E$ (GHz)	3.41(5)	2.77(2)	2.774(3)
$D + E$ (GHz)	−	4.373(1)	4.340(4)
D (GHz)	2.80(3)	2.993(1)	2.955(4)
E (GHz)	1.70(3)	1.382(3)	1.386(4)
k_x (s^{-1})	1.3(1)	0.65(2)	0.68(1)
k_y (s^{-1})	0.60(5)	0.45(2)	0.314(8)
k_z (s^{-1})	0.02(5)	0.03(5)	0.02(1)
R_{yx}	0.3(1)	0.16(5)	0.14(1)
R_{zx}	0.0(1)	0.00(5)	0.00(1)
W_{xy} (s^{-1})	0.00(1)	0.02(1)	0.062(3)
W_{xz} (s^{-1})	0.05(1)	0.03(1)	0.040(6)
W_{yz} (s^{-1})	0.05(1)	0.03(1)	0.041(2)

[a] Observed in SL3 DNA; k_{ave} fixed at 0.634 s^{-1} as found for guanosine. [b] Observed in SL3 DNA; k_{ave} fixed at 0.38 s^{-1}. [c] k_{ave} fixed at 0.338 s^{-1}.

equal, leading to very weak ODMR signals. Normally, the population of the highly radiative T_x sublevel of Trp is considerably smaller than those of the less radiative sublevels, T_y and T_z. This condition results in strong positive polarity (increases in phosphorescence intensity) ODMR signals. A major effect of aromatic stacking interactions with nucleic acids is enhanced selectivity of intersystem crossing (ISC) to T_x, which increases its stationary state population (*17*), thus decreasing, in general, the strength of the ODMR signals. In extreme cases, this can lead to stationary state Trp ODMR responses of negative polarity (*29*, *30*). The stationary state slow passage ODMR signals from complexes of NCp7 with SL3 DNA and with the *n*-nonane loop variant SL3$(CH_2)_9$ DNA are shown as traces A and C in Figure 5, respectively. Although the phosphorescence of the SL3 DNA complex of NCp7 is dominated by Trp (Figure 3C), its stationary state ODMR spectrum is weak, and appears to contain a significant adenine contribution at ∼1.7 GHz. The EEDOR spectrum (Figure 5B), saturating the 1.7 GHz region, reveals the $T_x \leftrightarrow T_y$ ($2E$) and $T_y \leftrightarrow T_z$ ($D + E$) signals of Trp37, which are seen to have negative polarity in contrast with the EEDOR signals of free NCp7 which are of positive polarity (Figure 4E). The EEDOR spectrum of the NCp7 complex of SL3$(CH_2)_9$ DNA, saturating the band at 1.7 GHz (Figure 5D), reveals a positive polarity Trp37 EEDOR

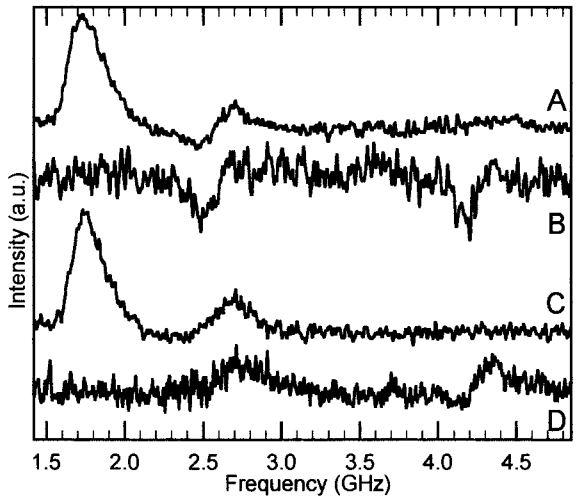

FIGURE 5: Steady state ODMR spectra of the 1:1 complex of NCp7 with SL3 DNA (A and B) and with $(CH_2)_9$SL3 DNA (C and D). Traces B and D are EEDOR spectra recorded during saturation of the low-frequency transitions of both adenine and tryptophan.

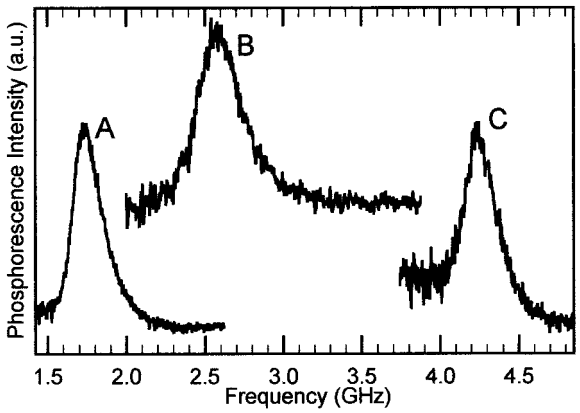

FIGURE 6: Delayed slow passage ODMR spectra of the NCp7−SL3 DNA complex. (A−C) Transitions $D - E$, $2E$, and $D + E$, respectively. Spectra A−C were obtained in separate experiments.

spectrum. This illustrates differences in the populating−depopulating dynamics of the Trp37 triplet state in the two complexes, leading to differences in relative steady state populations (n_i^0, where $i = x, y,$ or z). In the NCp7 complex with SL3 DNA, $^1/_2(n_x^0 + n_z^0) > n_y^0$, while the opposite is the case in the NCp7 complex with SL3$(CH_2)_9$ DNA. The delayed slow passage ODMR $D - E$ and $2E$ bands of Trp37 in each of the complexes could be separated from those of adenine because of the shorter lifetime of the adenine triplet state. The microwave frequency was swept through the Trp37 transitions after a sufficient time delay that no interference from adenine was evident. An example of the Trp37-delayed ODMR bands of the 1:1 NCp7−SL3 DNA complex is shown in Figure 6. The delayed ODMR signals are clearly far superior to those observed in the stationary state (Figure 5) because of significant spin alignment, not present in the stationary state, that develops during the decay. The results of the delayed slow passage measurements of the NCp7 complexes studied in this work are given in Table 2. The kinetic and radiative rate constants obtained from global analysis of MIDP data sets are given in Table 4.

Relative Sublevel Populating Rates. In previous work (*17*), we showed that the relative sublevel populating rates (P_i) of the Trp37 triplet state of NCp7 and its nucleic acid complexes could be obtained given the kinetic and radiative parameters that result from global MIDP analysis and the relative initial sublevel populations that also are obtained. The initial populations are assumed to equal the true stationary state populations in the analysis; this is strictly the case only for extremely long periods of excitation, but it can be shown that for our experimental conditions (15 s excitation) relatively small errors are introduced by this assumption and these are found largely for P_z, which is underestimated since T_z has the longest lifetime. The relative sublevel populating rates for Trp37 of NCp7 and its 1:1 SL complexes studied in this work are given in Table 4. Complex formation with oligonucleotides leads to significant increases of the P_x/P_y ratio, as was found in previous studies (*17*).

DISCUSSION

Fluorescence Titrations. The results of fluorimetric equilibrium binding isotherms of NCp7 with nucleic acids showed that the HIV-1 nucleocapsid protein can bind to both single- and double-stranded nucleic acid sequences. Electrostatic interactions with the phosphodiester backbone appear to contribute to a differing extent to the binding free energy of association of NCp7 to lattices of different strandedness.

In agreement with these findings, NCp7 was seen to display a 2:1 stoichiometry for binding to the various intact stem−loop sequences in their RNA and DNA forms. One binding center could be eliminated by removal of the nucleic acid bases from the loop region.

All stem−loop sequences bound NCp7 stoichiometrically under the conditions used in the ODMR studies. Addition of the cryosolvent resulted in only a minor change in the association constant. In general, RNA sequences exhibited comparable or somewhat higher affinity than their DNA counterparts, and mutations in the interactive G bases in the loop regions resulted in a reduction in binding affinity, in an additive fashion.

Interpretation of Phosphorescence Red Shifts and ZFS Shifts. The observation that complex formation with nucleic acids leads simultaneously to phosphorescence red shifts and ZFS changes of Trp37 suggests the use of a two-dimensional representation to characterize the interaction. In early ODMR studies (*31*−*34*), it was noted that these quantities were related. If the ODMR frequency was measured through an inhomogeneously broadened vibronic band (usually the 0,0-band) using narrow-band optical selection, a linear relationship between the phosphorescence red shift, $\Delta E_{0,0}$, and the ZFS shift, ΔD, is found. For quinoxaline in ethylene glycol/water glass (*35*) and naphthalene in 3-methylpentane glass (*34*), it is found that $\Delta D/\Delta E_{0,0} = 5.8 \times 10^{-6}$ and 5.0×10^{-6}, respectively. Both the red shift and the ZFS shift are attributed to local solvent perturbations that mix excited (and somewhat more diffuse) triplet states with the phosphorescent state. The ratios, above, are of the predicted sign and magnitude (*31*, *33*). A much larger ratio of $\Delta D/\Delta E_{0,0}$ is found (*36*, and references therein) for the naphthalene triplet state in naphthalenophanes in which two naphthalene moieties are joined face-to-face by bridging groups, forcing their π-orbitals to overlap. Both D and $E_{0,0}$ decrease with an increasing level of π-orbital interaction, yielding a slope $\Delta D/\Delta E_{0,0}$ of 15×10^{-6}. The large value of this ratio relative to that found

Table 4: Kinetic and Radiative Parameters of Trp37 in NCp7 and Its 1:1 Complexes with SL Structures[a]

substrate[b]	k_x (s^{-1})	k_y (s^{-1})	k_z (s^{-1})	R_{zx}[c]	R_{yx}[c]	W_{xy} (s^{-1})[d]	W_{xz} (s^{-1})[d]	W_{yz} (s^{-1})[d]	P_x[e]	P_y[e]
none	0.330(9)	0.117(5)	0.000(3)	0.000(9)	0.053(8)	0.04(1)	0.06(2)	0.05(3)	0.42	0.49
SL2 RNA	0.47(2)	0.13(1)	0.000(3)	0.00(2)	0.06(2)	0.03(1)	0.03(1)	0.075(3)	0.69	0.25
SL3 RNA	0.46(2)	0.11(1)	0.00(1)	0.00(2)	0.00(2)	0.06(1)	0.04(1)	0.052(2)	0.68	0.26
SL4 RNA	0.48(1)	0.105(7)	0.00(1)	0.00(1)	0.00(1)	0.055(6)	0.048(7)	0.043(1)	0.74	0.20
SL2 DNA	0.48(2)	0.17(1)	0.00(1)	0.01(2)	0.14(1)	0.00(1)	0.02(1)	0.061(2)	0.64	0.30
SL3 DNA	0.48(2)	0.10(1)	0.00(1)	0.00(2)	0.00(2)	0.04(1)	0.04(1)	0.038(2)	0.82	0.09
SL4 DNA	0.48(1)	0.113(6)	0.000(4)	0.00(1)	0.01(1)	0.046(5)	0.038(6)	0.047(1)	0.73	0.21
SL3(G7I) DNA	0.48(2)	0.109(8)	0.000(5)	0.00(1)	0.04(1)	0.030(7)	0.042(9)	0.042(1)	0.81	0.14
SL3(G9I) DNA	0.45(1)	0.109(5)	0.000(3)	0.000(8)	0.007(8)	0.046(4)	0.039(5)	0.0448(7)	0.76	0.18
SL3$(CH_2)_9$ DNA	0.48(2)	0.103(8)	0.000(5)	0.00(1)	0.00(1)	0.059(7)	0.049(8)	0.041(1)	0.75	0.19
SL3$(abasic)_4$ DNA	0.46(1)	0.108(8)	0.000(5)	0.00(1)	0.02(1)	0.044(7)	0.046(9)	0.047(1)	0.73	0.21
SL3$(abasic)_4$ DNA[f]	0.49(4)	0.09(1)	0.00(1)	0.00(2)	0.01(2)	0.05(2)	0.05(2)	0.045(3)	0.75	0.19
dsDNA	0.40(1)	0.101(6)	0.000(4)	0.00(1)	0.03(1)	0.027(5)	0.038(7)	0.0373(8)	0.77	0.17
ssDNA	0.42(2)	0.092(8)	0.003(5)	0.00(1)	0.00(1)	0.049(8)	0.04(1)	0.032(1)	0.86	0.09
SL2(U8BrU) DNA	0.46(1)	0.129(6)	0.000(4)	0.000(3)	0.00(1)	0.076(5)	0.042(6)	0.052(1)	0.69	0.25

[a] The estimated error in the last digit given in parentheses. [b] Excitation is at 297 nm except as noted. [c] R_{ix} is the radiative rate constant of T_i relative to T_x. [d] W_{ij} is the $T_i \leftrightarrow T_j$ spin−lattice relaxation rate constant. [e] Relative sublevel population rates. P_z is in the range of 0.04−0.09 but cannot be obtained accurately from the MIDP measurements. The estimated error in P_x and P_y is ±0.03. See the text. [f] Excitation is at 313 nm.

for naphthalene in 3-methylpentane glass (*34*) is attributed (*36*, and references therein) to the admixture of charge transfer character into the triplet state by transannular aromatic stacking interactions. Whereas solvent perturbations by aliphatic molecules are limited to Stark and local polarizability effects, an aromatic perturber can induce charge transfer character into the triplet state because it carries empty low-energy electron acceptor orbitals that are not present in aliphatic perturbing molecules. While only triplet states localized on the molecule are admixed by aliphatic molecules, delocalized (charge transfer) triplet states may be admixed by transannular stacking interactions with aromatic molecules. Although localized higher-energy triplet states are more diffuse than the phosphorescent state and their admixture leads to some reduction of D, the introduction of a comparable degree of charge transfer character leads to far greater reduction of the ZFS because of the r^{-3} dependence of the splittings (eqs 1 and 2).

For tryptophan in ethylene glycol/water glass, we find (*32*) $\Delta D/\Delta E_{0,0} = 3.7 \times 10^{-6}$. It is proposed that in the case of tryptophan interactions with nucleic acids, $\Delta D/\Delta E_{0,0}$ values in excess of that exhibited by interaction with aliphatic solvents (e.g., ethylene glycol/buffer mixtures) be considered an indication of aromatic stacking interactions with nucleic bases. The extent of mixing of the charge transfer triplet state, $^3\Psi_{CT}$, with the phosphorescent state, $^3\Psi_1$, will depend inversely on the energy splitting, ΔE_{CT}, which can be expressed for nucleic acid N as

$$E(^3\Psi_{CT}) - E(^3\Psi_1) = \Delta E_{CT} \approx \mathrm{IP(Trp)} - E_{0,0}\mathrm{(Trp)} - \mathrm{EA(N)} + C \quad (3)$$

where IP and EA are the vertical ionization energy and vertical electron affinity, respectively, and C consists of the Coulomb and polarization energy of the ion pair. A variable quantity on the right-hand side of eq 3 is EA, which differs for the nucleic bases. ΔE_{CT} will decrease with larger EA(N), and for a given degree of π-orbital overlap, the charge transfer character of $^3\Psi_1$ will increase and D will become smaller. To the extent that the phosphorescence red shift represents the degree of stacking (π-orbital interaction), the quantity $\Delta D/\Delta E_{0,0}$ may be characteristic of stacking with specific bases.

Experimental values for EA(N) are not available except for that for uracil which was found to have a gas phase vertical EA of −0.19 eV (*37*). Vertical gas phase EA values for the common bases have been calculated recently, however, using ab initio molecular orbital methods (*38*). The vertical EAs of the bases are found to increase in the order G < A < C < T < U, with values of −1.23, −0.74, −0.40, −0.32, and −0.19 eV, respectively. The adiabatic EA values of G and A are predicted to be negative as well, suggesting that G^- and A^- are unstable with respect to ionization in the vapor phase. The vertical IP of skatole has been measured to be 7.54 eV (*39*), which can be used for IP(Trp). C is estimated to be −3.0 eV, and $E_{0,0} = 3.0$ eV. Using these values in eq 3, we find that ΔE_{CT} lies between ∼1.7 eV for U and 2.8 eV for G. These estimated energy gaps are narrow enough that considerable mixing of $^3\Psi_{CT}$ with $^3\Psi_1$ is possible. Experimental values of $\Delta D/\Delta E_{0,0}$ are given in Table 2 for Trp37 in complexes of NCp7 with the oligonucleotides investigated in this work.

Estimate of the Limiting Value of $\Delta D/\Delta E_{0,0}$. Since it is apparent that the admixture of a charge transfer triplet state will lead to far greater reduction of D than an equal admixture of a localized triplet state, it will be assumed that the *maximum* value of this ratio will occur if both ΔD and $\Delta E_{0,0}$ result from the admixture of a single low-lying charge transfer state by transannular π-electron interactions.

$\Delta E_{0,0}$ is the difference in the energy shift between the phosphorescent state and the ground state due to the interaction. The zero-order charge transfer triplet state, $^3\Psi_{CT}^{(0)}$, and the corresponding singlet state, $^1\Psi_{CT}^{(0)}$, will mix with the zero-order phosphorescent state, $^3\Psi_1^{(0)}$, and ground state, $^1\Psi_0^{(0)}$, respectively. To second order in perturbation theory,

$$\Delta E_{0,0} = -|\langle V_{int}\rangle_{TT}|^2/\{E[^3\Psi_{CT}^{(0)}] - E[^3\Psi_1^{(0)}]\} + |\langle V_{int}\rangle_{SS}|^2/\{E[^1\Psi_{CT}^{(0)}] - E[^1\Psi_0^{(0)}]\} \quad (4)$$

where $\langle V_{int}\rangle_{TT}$ and $\langle V_{int}\rangle_{SS}$ are matrix elements of the transannular interaction potential. V_{int} is independent of spin variables; therefore, it can only mix states of the same multiplicity. Consistent with our level of approximation, we will assume that the singlet and triplet matrix elements are

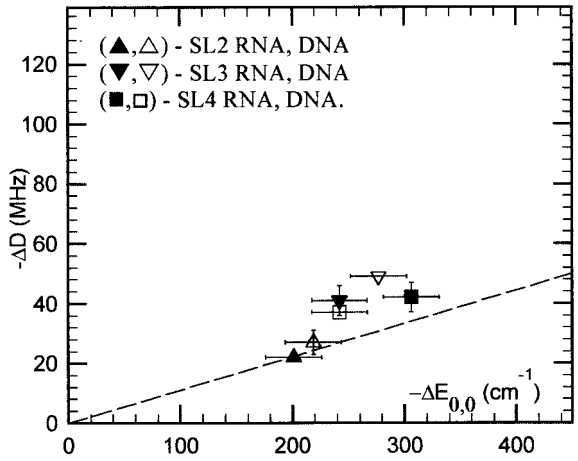

FIGURE 7: Zero-field splitting ($-\Delta D$) vs the red shift ($-\Delta E_{0,0}$) of NCp7 complexes with SL structures (see the legend). The dashed line has a dimensionless slope of 3.7×10^{-6}.

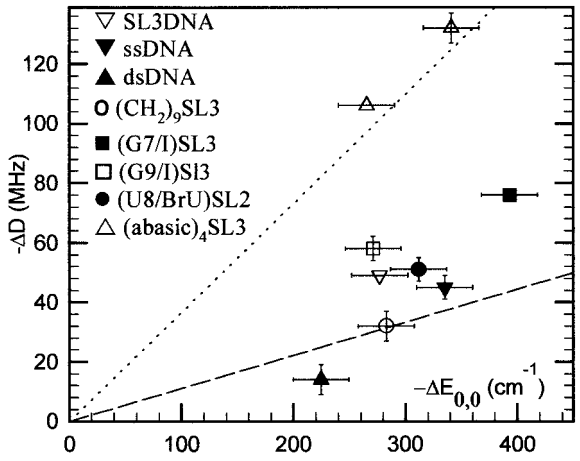

FIGURE 8: Zero-field splitting ($-\Delta D$) vs the red shift ($-\Delta E_{0,0}$) of NCp7 complexes with DNA structures (see the legend). The dashed line has a slope of 3.7×10^{-6}, and the dotted line has a slope of 12×10^{-6}.

approximately equal, since ${}^3\Psi_{CT}{}^{(0)}$ and ${}^1\Psi_{CT}{}^{(0)}$ differ only in electron spin and the main configurations of ${}^3\Psi_1{}^{(0)}$ (${}^3L_a$) and ${}^1\Psi_0{}^{(0)}$ vary by a single electron orbital (*40*). The energies of ${}^3\Psi_{CT}{}^{(0)}$ and ${}^1\Psi_{CT}{}^{(0)}$ differ by $2J$, where J is the exchange energy. If it is assumed that J can be neglected relative to the energy denominators of eq 4, this equation becomes

$$\Delta E_{0,0} \approx |\langle V_{int}\rangle|^2[-1/\Delta E_{CT} + 1/(E_{0,0} + \Delta E_{CT})] \quad (5)$$

where $\Delta E_{CT} = E[{}^3\Psi_{CT}{}^{(0)}] - E[{}^3\Psi_1{}^{(0)}]$. To first order, the normalized phosphorescent state wave function is

$${}^3\Psi_1{}^{(1)} = (1 - |\alpha|^2)^{1/2}{}^3\Psi_1{}^{(0)} - \alpha\,{}^3\Psi_{CT}{}^{(0)} \quad (6)$$

where overlap of ${}^3\Psi_{CT}{}^{(0)}$ with ${}^3\Psi_1{}^{(0)}$ is ignored and $\alpha = \langle V_{int}\rangle/\Delta E_{CT}$. Since the contribution of ${}^3\Psi_{CT}{}^{(0)}$ to $D^{(1)} = {}^3/_4(\gamma\hbar)^2$-$\langle {}^3\Psi_1{}^{(1)}|(r_{12}{}^2 - 3z_{12}{}^2)/r_{12}{}^5|{}^3\Psi_1{}^{(1)}\rangle$ may be neglected because of the effective $r_{12}{}^{-3}$ dependence of the operator, it follows that

$$D^{(1)} - D^{(0)} = \Delta D \approx -|\alpha|^2 D^{(0)} \quad (7)$$

where $D^{(0)}$ is the ZFS parameter in the absence of stacking.

Combining eqs 5 and 7 gives

$$(\Delta D/\Delta E_{0,0})_{max} \approx D^{(0)}(1/\Delta E_{CT} + 1/E_{0,0}) \quad (8)$$

Using ΔE_{CT} estimated from eq 3, a $D^{(0)}$ value of 9.8×10^{-2} cm^{-1}, and an $E_{0,0}$ value of 2.5×10^4 cm^{-1}, we find $(\Delta D/\Delta E_{0,0})_{max} \approx 11 \times 10^{-6}$ for U and 8×10^{-6} for G. The estimated value of $(\Delta D/\Delta E_{0,0})_{max}$ for U agrees closely with the measured ratio (*17*) for the NCp7 complex with poly(U), 12×10^{-6}, suggesting that admixing of charge transfer states by transannular π-electron interactions plays an important role in this complex. On the other hand, $(\Delta D/\Delta E_{0,0})_{max}$ estimated for G is significantly larger than 2.0×10^{-6}, the experimental ratio (*17*) for the NCp7 complex of dG_8, suggesting that charge transfer state mixing does not play an important role in this complex.

Representation of ΔD versus $\Delta E_{0,0}$ for NCp7−SL Complexes. The values of ΔD are plotted against $\Delta E_{0,0}$ in Figure 7 for the DNA and RNA SL complexes reported in this work. Also shown in Figure 7 is a line with a slope of 3.7×10^{-6}, which represents the $\Delta D/\Delta E_{0,0}$ ratio expected for tryptophan undergoing solvent shifts in the absence of aromatic stacking interactions. The data points for SL2 RNA and DNA fall close to this line, indicating that charge transfer character induced by transannular π-electron interactions does not play an important role in these complexes. The NMR structures of the NCp7−SL3 RNA complex (*18*) and of its SL2 RNA complex (*41*) reveal the close approach of Trp37 to G7 of the tetraloop (Figure 2) in each case. $\Delta D/\Delta E_{0,0}$ values for the SL3 RNA and DNA complexes have a ratio of $>3.7 \times 10^{-6}$, suggesting that interaction with guanine introduces charge transfer via aromatic stacking. The ratio is considerably less than 8×10^{-6}, however, the maximum estimated for guanine in the previous section, so we believe that localized triplet states are admixed as well. Interaction with G7 of the SL2 tetraloop apparently involves weaker stacking interactions of Trp37 than with the SL3 tetraloop. We find that the data point of the SL3 DNA complex is in the same position, within experimental error, as that of the NCp7 complex with $d(TG)_4$ (*17*), suggesting a similar type of interaction with guanine in the two complexes. The $\Delta D/\Delta E_{0,0}$ ratios exhibited by SL4 RNA and DNA are intermediate between those of the SL2 and SL3 complexes. If the structure of the complex is similar to that observed for SL3 RNA (*18*) or SL2 RNA (*41*), the nearest approach of Trp37 would be to the adenine that occupies position 7 of the SL4 loop. NCp7, however, produces extremely small ΔD and $\Delta E_{0,0}$ values in binding to poly(A) (*17*), so a different binding mode with SL4 is likely. The red shifts of all the SL complexes fall in the range of 200−300 cm^{-1}, which appears to be characteristic of NCp7 interactions with guanine-containing oligonucleotides (*17*). On the other hand, NCp7 binding to poly(I) and inosine-containing oligonucleotides produces red shifts of >350 cm^{-1}, while in complexes with poly(U) and poly(dT), we find red shifts of <150 cm^{-1} (*17*).

The ΔD versus $\Delta E_{0,0}$ data for NCp7 complexes of the mutated SL sequences and SL variants are plotted in Figure 8 along with data from the ssDNA and dsDNA oligomers. The SL3 DNA complex is included, as well, to provide a reference. Shown in Figure 8 are a line with a slope of 3.7×10^{-6} and one with a slope of 12×10^{-6}, the value of $\Delta D/\Delta E_{0,0}$ measured (*17*) for NCp7 complexed with poly(U). The data for ssDNA and dsDNA suggest that charge transfer character resulting from stacking is present in the

former, while the latter shows no effects of aromatic stacking. The very small value of $\Delta D/\Delta E_{0,0}$ for the dsDNA complex, similar to that exhibited by NCp7 complexes of rG_8 and dG_8, suggests the possibility of an edge-on interaction, rather than stacking of Trp37 with a nucleobase. A large red shift is found for the NCp7 complex of SL3(G7I) DNA relative to the native SL3 DNA complex. On the other hand, the complex with the SL3(G9I) mutant has the same red shift as the native SL3 DNA complex. The datum for the NCp7 complex of SL3(G7I) is identical within experimental error to that observed previously (*17*) for the NCp7 complex of dI_8, suggesting a similar interaction with the hypoxanthine base. These results provide strong evidence for an interaction between Trp37 and G7 in the SL3 complex, in agreement with the NMR structure (*18*). In the G9I mutant, a hydrogen bond between G6 and G9 is lost. The resulting relaxation of the loop structure could allow an increased level of aromatic stacking between Trp37 and G7, producing a $\Delta D/\Delta E_{0,0}$ (7.1×10^{-6}) in this complex somewhat larger than that found in the native SL3 complex (5.9×10^{-6}). The complex of NCp7 with the SL2(U8BrU) mutant exhibits a significant red shift relative to the native SL2 complex, but there is no heavy atom effect revealed by the sublevel lifetimes (Table 4). This indicates that Trp37 does not approach to make van der Waals contact with BrU at position 8, in agreement with the NMR structure of the NCp7−SL2 RNA complex (*41*); the enhanced red shift possibly results from the polarizability of the Br atom which should be nearby. The larger value of $\Delta D/\Delta E_{0,0}$ relative to that of the SL2 complex suggests that aromatic stacking is enhanced as a consequence of structural alterations induced by the bulky Br atom. We should caution that our discussion based on the NMR structure of the SL2 complex (*41*) contains the implicit assumption that the A-bulge, present in the SL2 stem (Figure 1) and incorporated in the construct used in the structural work (*41*) but absent in our sample, has little influence on the structure of the complex in the vicinity of Trp37.

Two variants of SL3 devoid of loop bases were investigated to determine the effects on NCp7 of binding to the stem region. As discussed above, $SL3(CH_2)_9$ and SL3(apurinic)$_4$ bind NCp7 with 1:1 stoichiometries, while the variants with their loop bases intact bind with 2:1 stoichiometries. Surprisingly, $SL3(CH_2)_9$ and SL3(apurinic)$_4$ complexes revealed widely different interactions of the Trp37 probe despite their identical stem sequences. The shifts observed with $SL3(CH_2)_9$ binding are intermediate between those observed for dsDNA and ssDNA (Figure 8), indicating only minor, if any, charge transfer character induced by aromatic stacking. In contrast, complex formation between NCp7 and SL3(apurinic)$_4$ produced an extremely large value of $\Delta D/\Delta E_{0,0}$ (Table 2 and Figure 8). The energy levels of our samples are subject to inhomogeneous broadening because of a distribution of structures. Using normal and red edge excitation, we were able to select two triplet state populations of the NCp7−SL3(apurinic)$_4$ complex with differing red shifts and ZFS shifts (Table 2 and Figure 8). As can be seen in Figure 8 and Table 2, the points representing each of these populations have the same slope, $\Delta D/\Delta E_{0,0}$, thus demonstrating the validity of the correlation between the red shift and the ZFS shift for a single complex. The two optically selected populations represent different degrees of aromatic stacking between Trp37 and stem base(s). From the value of $\Delta D/\Delta E_{0,0}$, which is effectively the same as observed previously (*17*) for the poly(U) complex and greater than the maximum value estimated above for a G interaction, stacking with U is suggested. The red shift of the NCp7 complex with SL3(apurinic)$_4$ is much greater than that of the poly(U) complex, however, indicating a larger degree of transannular π-electron interactions.

We suggest that the differing modes of binding of NCp7 to $SL3(CH_2)_9$ and SL3(apurinic)$_4$ are determined by the loop structure which is compact and hydrophobic in the former and more open and hydrophilic in the latter. Thus, if binding of the zinc finger sequences of NCp7 to an open single-stranded DNA structure is energetically more favorable than binding to a closed duplex structure, the former mode of binding can be achieved at less energy cost with SL3(apurinic)$_4$ than with $SL3(CH_2)_9$.

Effects of Complex Formation on Kinetics. The formation of each nucleic acid complex by NCp7 is accompanied by changes in the kinetics of the Trp37 triplet state. The data in Table 4 reveal that nucleic acid binding causes an increase in k_x that ranges between 20 and 50% depending on substrate, while k_y and k_z are less affected. Also, the intersystem crossing pattern undergoes similar effects, with a large relative increase in P_x being produced. These effects are consistent with enhanced spin−orbit coupling of the triplet state with singlet states that emphasizes the T_x sublevel. We will now consider a mechanism that may partially explain these observations.

In $^3(\pi,\pi^*)$ states of planar aromatic molecules such as indole, spin−orbit coupling (SOC) with singlet states that leads to intersystem crossing (ISC) is very inefficient, and normally is most effective in the in-plane sublevels, T_x and T_y. However, they mix to only a small degree with high-energy $^1(\sigma,\pi^*)$ and $^1(\pi,\sigma^*)$ configurations (*27*, *28*). Thus, triplet sublevel lifetimes are long, with T_z having the longest, as we find for indole. The inefficiency of SOC results largely from the planar symmetry of the aromatic molecule in which there is rigorous separation of σ and π orbitals. It was suggested some time ago by El-Sayed et al. (*42*) that enhancement of SOC can result from *static distortions that effectively remove the symmetry plane of an aromatic molecule,* allowing for the direct mixing of σ and π orbitals. Such distortions are predicted to selectively enhance SOC in the in-plane sublevels. There is experimental evidence that aromatic stacking interactions, as found in charge transfer complexes, lead to reduced triplet state lifetimes as well as to enhanced ISC (*43*, *44*). Enhancement of ISC in proflavin when complexed with DNA has been observed by Lee and Galley (*45*), who suggested that an increased triplet yield might be responsible for fluorescence quenching by DNA in this system. Thus, we suggest that the interaction between Trp37 and a base in the NCp7 complexes with the SL structures induces an *asymmetric distortion* with the subsequent loss of the symmetry plane of indole. In this connection, it is interesting to note that in recent studies of polynucleotide complexes of small tetrapeptides containing tryptophan (*46*), we find large values of ΔD and $\Delta E_{0,0}$ that are consistent with aromatic stacking interactions with a significant charge transfer component. In these complexes, however, we see essentially no effect of enhanced SOC. We suggest that the enhancement of kinetics results from *asymmetric* interactions with bases that are imposed on Trp37

of NCp7 by the restricted configurational space dictated by the zinc finger structure. The tetrapeptides, on the other hand, have a great deal more configurational flexibility, and the tryptophan may be free to interact with the bases in a more symmetrical manner, i.e., by intercalation between bases rather than interacting asymmetrically with a single base.

NOTE ADDED IN PROOF

We emphasize that our estimate of $(\Delta D/\Delta E_{0,0})_{max}$ in this paper is based on an interaction model in which only a single charge transfer state dominates the perturbation. Situations may occur in which localized states are admixed by specific interactions that produce significant lowering of the ground state energy of Trp, leading to small or even positive $\Delta E_{0,0}$. Thus, large (or even negative) values of $\Delta D/\Delta E_{0,0}$ may be found that are not associated with aromatic stacking or charge transfer. These interactions should be characterized, however, by relatively small magnitudes of $\Delta E_{0,0}$.

REFERENCES

1. Coffin, J. M. (1992) in *The Retroviridae* (Levy, J. A., Ed.) Vol. 1, pp 19−50, Plenum Press, New York.
2. Luciv, P. A. (1992) in *The Retroviridae* (Levy, J. A., Ed.) Vol. 1, pp 159−298, Plenum Press, New York.
3. Darlix, J.-L., Lapadat-Tapolsky, M., de Rocquigny, H., and Roques, B. P. (1995) *J. Mol. Biol. 254*, 523−537.
4. Lever, A. M., Göttlinger, H. G., Haseltine, J. G., and Sodroski, J. G. (1989) *J. Virol. 63*, 4085−4087.
5. Karpel, R. L., Henderson, L. E., and Oroszlan, S. (1987) *J. Biol. Chem. 262*, 4961−4967.
6. Berg, J. (1986) *Science 232*, 485−487.
7. Bess, J. W., Jr., Powell, P. J., Issaq, H. J., Schumack, L., Grimes, M. K., Henderson, L. E., and Arthur, L. O. (1992) *J. Virol. 66*, 840−847.
8. Gorelick, R. J., Henderson, L. E., Hanser, J. P., and Rein, A, (1988) *Proc. Natl. Acad. Sci. U.S.A. 85*, 8420−8424.
9. Gorelick, R. J., Chabot, D. J., Ott, D. E., Gagliardi, T. D., Rein, A., Henderson, L. E., and Arthur, L. O. (1996) *J. Virol. 70*, 2593−2597.
10. Aldovini, A., and Young, R. A. (1990) *J. Virol. 64*, 1920−1926.
11. De Rocquigny, H., Ficheux, D., Gabus, C., Allain, B., Fournie-Zaluski, M. C., Darlix, J. L., and Roques, B. P. (1993) *Nucleic Acids Res. 21*, 823−829.
12. Housset, V., De Rocquigny, H., Roques, B. P., and Darlix, J. L. (1993) *J. Virol. 67*, 2537−2545.
13. Gorelick, R. J., Benveniste, R. E., Gagliardi, T. D., Wiltrout, T. A., Busch, L. K., Bosche, W. J., Coren, L. V., Lifson, J. D., Bradley, P. J., Henderson, L. E., and Arthur, L. O. (1999) *Virology 253*, 259−270.
14. Méric, C., and Goff, S. P. (1989) *J. Virol. 63*, 1558−1568.
15. Berkowitz, R. D., Ohagen, A., Hoglund, S., and Goff, S. P. (1995) *J. Virol. 69*, 6445−6546.
16. Lam, W.-C., Maki, A. H., Casas-Finet, J. R., Erickson, J. W., Sowder, R. C., II, and Henderson, L. E. (1994) *Biochemistry 33*, 10693−10700.
17. Wu, J. Q., Ozarowski, A., Maki, A. H., Urbaneja, M. A., Henderson, L. E., and Casas-Finet, J. R. (1997) *Biochemistry 36*, 12506−12518.
18. De Guzman, R. N., Wu, Z. R., Stalling, C. C., Pappalardo, L., Borer, P. N., and Summers, M. F. (1998) *Science 279*, 384−388.
19. Wu, J. Q., Ozarowski, A., and Maki, A. H. (1996) *J. Magn. Reson., Ser. A 119*, 82−89.
20. Ozarowski, A., Wu, J. Q., and Maki, A. H. (1996) *J. Magn. Reson., Ser. A 121*, 178−186.
21. Wu, J. Q., Ozarowski, A., Davis, S. K., and Maki, A. H. (1996) *J. Phys. Chem. 100*, 11496−11503.
22. Ozarowski, A., and Maki, A. H. (2000) *J. Phys. Chem. B 104*, 1122−1127.
23. Smith, C. A., and Maki, A. H. (1993) *J. Phys. Chem. 97*, 997−1003.
24. Kwiram, A. L. (1982) in *Triplet State ODMR Spectroscopy* (Clarke, R. H., Ed.) pp 427−478, Wiley-Interscience, New York.
25. Hoover, R. J., Luk, K. F. S., and Maki, A. H. (1974) *J. Mol. Biol. 89*, 363−378.
26. McGlynn, S. P., Azumi, T., and Kinoshita, M. (1969) *Molecular Spectroscopy of the Triplet State*, Prentice-Hall, Englewood Cliffs, NJ.
27. Weissman, S. I. (1950) *J. Chem. Phys. 18*, 232−233.
28. McClure, D. S. (1952) *J. Chem. Phys. 20*, 682−686.
29. Khamis, M. I., Casas-Finet, J. R., Maki, A. H., Murphy, J. B., and Chase, J. W. (1987) *J. Biol. Chem. 262*, 10938−10945.
30. Zang, L.-H., Maki, A. H., Murphy, J. B., and Chase, J. W. (1987) *Biophys. J. 52*, 867−872.
31. Van Egmond, J., Kohler, B. E., and Chan, I. Y. (1975) *Chem. Phys. Lett. 34*, 423−426.
32. Von Schütz, J. U., Zuclich, J., and Maki, A. H. (1974) *J. Am. Chem. Soc. 96*, 714−718.
33. Williamson, R. L., and Kwiram, A. L. (1988) *J. Chem. Phys. 88*, 6092−6106.
34. Gradl, G., Friedrich, J., and Kohler, B. E. (1986) *J. Chem. Phys. 84*, 2079−2083.
35. Alfredson, T. V., Maki, A. H., and Waring, M. J. (1991) *Biochemistry 30*, 9665−9675.
36. Haenel, M. W., and Schweitzer, D. (1988) *Adv. Chem. Ser. 217*, 333−355.
37. Compton, R. N., Yoshioka, Y., and Jordan, K. D. (1980) *Theor. Chim. Acta 54*, 259−260.
38. Sevilla, M. D., Besler, B., and Colson, A.-O. (1995) *J. Phys. Chem. 99*, 1060−1063.
39. Lias, S. G., Bartmess, J. E., Liebman, J. F., Holmes, J. L., Levin, R. D., and Mallard, W. G. (1988) *J. Phys. Chem. Ref. Data 17* (Suppl. 1), 390.
40. Callis, P. R. (1997) *Methods Enzymol. 278*, 113−150.
41. Amarasinghe, G. K., De Guzman, R. N., Turner, R. B., Chancellor, K. J., Wu, Z. R., and Summers, M. F. (2000) *J. Mol. Biol. 301*, 491−511.
42. El-Sayed, M. A., Moomaw, W. R., and Chodak, J. B. (1973) *Chem. Phys. Lett. 20*, 11−16.
43. Czekalla, J., Briegleb, G., Herre, W., and Vahlensieck, H. J. (1959) *Z. Elektrochem. 63*, 715−724.
44. Christodouleas, N., and McGlynn, S. P. (1964) *J. Chem. Phys. 40*, 166−174.
45. Lee, W. E., and Galley, W. C. (1988) *Biophys. J. 54*, 627−635.
46. Misra, A., Ozarowski, A., Casas-Finet, J. R., and Maki, A. H. (2000) *Biochemistry 39*, 13772−13780.

BI002010I